Solid State Electronics xxx (xxxx) xxx–xxx

Contents lists available at ScienceDirect

Solid State Electronics

journal homepage: www.elsevier.com/locate/sse

The electron trap parameter extraction-based investigation of the relationship between charge trapping and activation energy in IGZO TFTs under positive bias temperature stress

Jihyun Rhee, Sungju Choi, Hara Kang, Jae-Young Kim, Daehyun Ko, Geumho Ahn, Haesun Jung, Sung-Jin Choi, Dong Myong Kim, Dae Hwan Kim*

School of Electrical Engineering, Kookmin University, Seoul 02707, Republic of Korea

ARTICLE INFO

Keywords:
Electron trap in gate insulator
Parameter extraction
IGZO TFT
PBTS instability
Charge trapping
Activation energy

ABSTRACT

Experimental extraction of the electron trap parameters which are associated with charge trapping into gate insulators under the positive bias temperature stress (PBTS) is proposed and demonstrated for the first time in amorphous indium-gallium-zinc-oxide thin-film transistors. This was done by combining the PBTS/recovery time-evolution of the experimentally decomposed threshold voltage shift (ΔV_T) and the technology computer-aided design (TCAD)-based charge trapping simulation. The extracted parameters were the trap density (N_{OT}) = $2.6 \times 10^{18}\,cm^{-3}$, the trap energy level (ΔE_T) = 0.6 eV, and the capture cross section (σ_0) = $3 \times 10^{-19}\,cm^2$.

Furthermore, based on the established TCAD framework, the relationship between the electron trap parameters and the activation energy (E_a) is comprehensively investigated. It is found that E_a increases with an increase in σ_0, whereas E_a is independent of N_{OT}. In addition, as ΔE_T increases, E_a decreases in the electron trapping-dominant regime (low ΔE_T) and increases again in the Poole–Frenkel (PF) emission/hopping-dominant regime (high ΔE_T). Moreover, our results suggest that the cross-over ΔE_T point originates from the complicated temperature-dependent competition between the capture rate and the emission rate. The PBTS bias dependence of the relationship between E_a and ΔE_T suggests that the electric field dependence of the PF emission-based electron hopping is stronger than that of the thermionic field emission-based electron trapping.

1. Introduction

Amorphous indium-gallium-zinc-oxide (a-IGZO) thin-film transistors (TFTs) were successfully employed in the backplane for large-screen organic light-emitting diode (OLED) displays and liquid-crystal displays (LCDs) [1,2]. These transistors were used because of their beneficial properties such as good uniformity over large areas, low processing temperatures, low-cost fabrication, compatibility with flexible substrates, and fair mobility [3,4]. Recently, the a-IGZO TFTs have been used in flexible processors, programmable units, and sensor-embedded wearable circuitry for wearable healthcare and the Internet-of-things era [5–7]. However, reliability issues, as technological challenges for more successful mass production and commercialization of IGZO TFTs, still remain.

Among the reliability issues, positive bias temperature stress (PBTS)-induced instability is very important because the PBTS corresponds to the ON condition of n-channel IGZO TFTs. Actually, current-driving TFTs in an OLED pixel and TFTs in the gate-driver circuitry are often under the influence of PBTS. Very recently, the PBTS instability of IGZO TFT was experimentally decomposed into the defect creation in the active layer and electron-charge trapping in the gate insulator (GI) [8]. Here it is worthwhile to note that the latter depends on the GI quality that varies significantly corresponding to the process or according to the GI material chosen for the fabrication, whereas the former is somewhat entangled with intrinsically IGZO material issues and thus frequently analyzed in *ab initio* studies [9–11]. Nevertheless, compared with the defect creation in active layers, the PBTS-induced electron trapping in IGZO TFTs has been less investigated quantitatively despite its importance for wearable circuits.

In particular, the detailed procedure of extracting the physical parameters for GI electron trap, such as spatial density, capture cross section, charge emission rate, and energy level, from the measured stress time-evolution of threshold voltage (V_T) has been rarely investigated in IGZO TFTs in spite of its practical importance. Even in an

* Corresponding author.
E-mail address: drlife@kookmin.ac.kr (D.H. Kim).

http://dx.doi.org/10.1016/j.sse.2017.10.024

extremely small numbers of previous studies on GI trap parameter in TFTs [12–14], the values of trap parameters have been found to be in a variety of ranges; 1.59×10^{18}–4.17×10^{18} [cm^{-3}] (spatial density), 0.2–2.24 eV (energy level), and 3×10^{-22}–1×10^{-15} cm^2 (capture cross section).

More importantly, the measured stress time-evolution of V_T includes contribution factor due to the charge trapping into GI as well as the defect creation in active film, which makes it more difficult to exactly extract the GI electron trap parameters from the experimental data. Accuracy of the GI trap parameters should be very carefully dealt in terms of the process optimization and reliability improvement because erroneous values of the GI trap parameters can mislead one to wrong conclusion or faulty engineering direction. Therefore, the de-embedded V_T shift (ΔV_T), i.e., the ΔV_T associated only with the charge trapping into GI, needs to be used as the experimental PBTS-induced ΔV_T data when the extraction of GI trap parameter is performed. However, this approach has been rarely demonstrated because the experimental technique for decomposing the PBTS ΔV_T into respective instability mechanisms was proposed very recently [8].

In this paper, experimental extraction of the GI electron trap parameters which are only associated with charge trapping into GI under PBTS is proposed and its detailed procedure is demonstrated for the first time in a-IGZO TFTs. Our extraction technique is based on well-calibrated technology computer-aided design (TCAD) framework. Our parameters and TCAD simulation reproduced the measured PBTS time-evolution of ΔV_T very well over a wide range of temperatures. Furthermore, relationship between the electron trap parameters and the activation energy (E_a) is comprehensively investigated. We found that E_a increases with an increase in σ_0, whereas E_a is independent of N_{OT}. In addition, the electron trapping-dominant regime and the Poole-Frenkel (PF) emission/hopping-dominant regime were comparatively analyzed.

2. Device fabrication and characterization

The a-IGZO TFTs with the inverted staggered bottom-gate top-etch stopper (ES) structure were fabricated on a glass substrate as shown in Fig. 1(a). The detailed process is as follows. A molybdenum was deposited on the glass substrate using an rf sputtering process, and it was patterned by dry etching. Then, the GI made up of a 100-nm-thick SiO_2 layer was deposited by plasma-enhanced chemical-vapor-deposition (PECVD). The 50-nm-thick a-IGZO thin-film was DC sputter-deposited under 3 kW at room temperature in a gas mixture of Ar/O_2 = 35/63 at sccm; here, the atomic ratio was In:Ga:Zn = 2:2:1. The active layer was then patterned by wet etching with diluted HF solution. Subsequently, the 100-nm-thick SiO_2 was formed as the ES layer by PECVD and dry etch patterning. Molybdenum was then dc sputter-deposited and patterned by dry etching as the source/drain (S/D) electrodes. Subsequently, the 100-nm-thick SiO_2 was PECVD-deposited as a passivation layer. Lastly, the post-annealing process was performed at 250 °C for one hour.

Geometrical parameters are as follows. The oxide thickness of GI (T_{GI}) was 100 nm, the active layer thickness (T_{IGZO}) was 50 nm, the channel length (L) was 50 μm, the gate-to-S/D overlap length (L_{OV}) was 15 μm, and the channel width (W) was 25 μm.

The V_T was taken from the measured I-V characteristics, which were characterized using the HP4156 semiconductor parameter analyzer. V_T was measured during PBTS for 10^4 s and during the recovery period for additional 2×10^4 s. Here, the PBTS condition was the gate-to-source voltage (V_{GS}) = 30 V and the drain-to-source voltage (V_{DS}) = 0 V; the recovery condition was $V_{GS} = V_{DS} = 0$ V, when the temperature was varied from 300 to 373 K. Among the physical mechanisms of the PBTS-induced ΔV_T, the contribution factor only due to the electron trapping into GI was experimentally decomposed using the method in [8]; this de-embedded ΔV_T factor is shown as triangles in Fig. 2(a) and (b). Details of de-embedding ΔV_T is given in [8].

3. Parameter extraction

The cross section and the energy band at a flat band voltage ($V_{GS} = V_{FB}$) condition of the bottom-gate a-IGZO TFT are illustrated in Fig. 1(b) and (c). The physical parameters of GI electron trap can be summarized as its spatial density N_{OT} [cm^{-3}], capture cross section σ_0 [cm^2], and energy level E_T [eV], respectively. As shown in Fig. 1(c), the energy level E_T of electron trap is defined by ΔE_T [eV] which means the separation above the IGZO conduction band minimum ($E_{C,IGZO}$). For simplicity, we assume that the electron trap in GI is located in a single energy level. i.e., ΔE_T above $E_{C,IGZO}$.

In order to establish the procedure of extracting all of N_{OT}, σ_0, and ΔE_T from the experimentally de-embedded ΔV_T, first of all, the framework of TCAD simulation was set up by using the Atlas-2D of Silvaco [15]. The Fowler-Nordheim tunneling, band-to-band tunneling, trap-assisted tunneling, and the Poole-Frenkel (PF) emission were incorporated into TCAD simulation. Here, it should be noted that all of N_{OT}, σ_0, and ΔE_T are TCAD-compatible parameters.

Given the stress bias (V_{STR}) applied to V_{GS} and the temperature (T), the PBTS/recovery time-evolution of the de-embedded ΔV_T is shown by triangles in Fig. 2(a) and (b). Here, we define the $\Delta V_{T,rec}$ and $t_{sat,rec}$ as the fast recoverable ΔV_T factor during recovery period and as the time when $|d\Delta V_T/dt|$ becomes lower than 10 μV/s, as schematically illustrated in Fig. 3(a). Then, $\Delta V_{T,rec}$ and $t_{sat,rec}$ will be distinct functions of N_{OT}, σ_0, and ΔE_T as well as of V_{STR} and T. If a clear pattern exists in these functional relationships, we would be able to use those patterns in extracting parameters, such as N_{OT}, σ_0 and ΔE_T because $\Delta V_{T,rec}$ and $t_{sat,rec}$ can be characterized experimentally under given V_{STR} and T conditions.

In order to find out the pattern between the trap parameters, such as

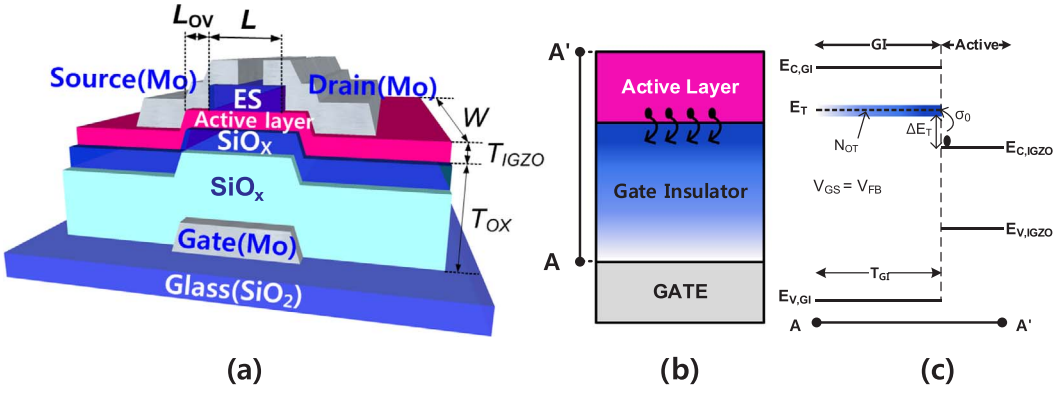

Fig. 1. (a) Bottom-gate IGZO TFT structure. (b) Schematic cross section of bottom-gate a-IGZO TFTs. (c) Energy band structure of IGZO TFTs at the interface of active layer and gate insulator under the flat band condition.

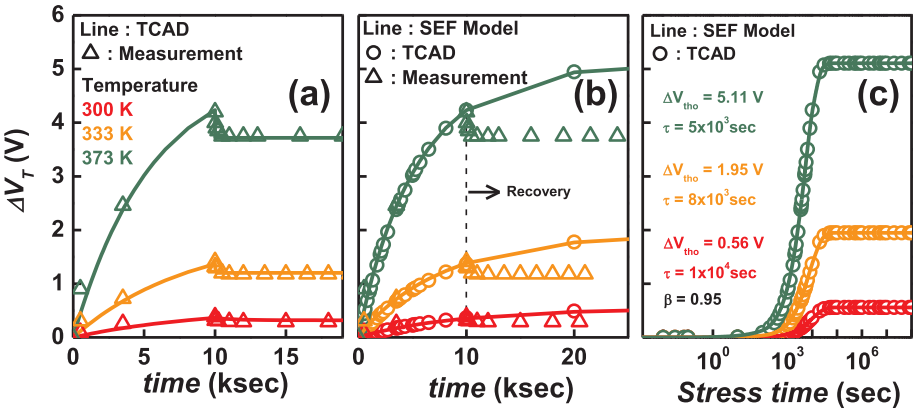

Fig. 2. Time evolution of ΔV_T during the PBS/recovery time with different temperatures. (a) Reproduction of measurement data through the TCAD. SEF model fitting of (b) TCAD and measurement data to relatively short time in linear-time scale, (c) TCAD up to ΔV_T saturation time in log-time scale.

N_{OT}, σ_0 and ΔE_T, and the $\Delta V_{T,rec}$ and $t_{sat,rec}$, the TCAD simulation was performed with varying T = 300, 333, and 373 K. From our simulation results, interestingly, three patterns were clearly observed in terms of the normalized $t_{sat,rec}(T)$, e.g., $t_{sat,rec}(T)/t_{sat,rec}(T = 373\,K)$; (1) the normalized $t_{sat,rec}(T)$ is independent of N_{OT} (Fig. 4(a)), (2) it is also independent of σ_0 (Fig. 4(b)), and (3) it is linearly proportional to ΔE_T and its slope increases as T increases (Fig. 4(c)). Therefore, the GI trap parameters can be extracted by comparing the experimentally characterized parameters, such as the $t_{sat,rec}(T)$ normalized at 373 K, $t_{sat,rec}$ itself, and $\Delta V_{T,rec}$, with the simulated ones at various temperatures.

Fig. 3(b) explains the procedure of parameter extraction. Details are as follows. First of all, the fundamental input parameters including the effective density-of-states (N_C and N_V), band mobility (μ_{Band}), and doping concentration (N_{SD}) are adopted with the PF emission rate factor (PF.B) which will be shown later in Eq. (3). In this step, N_C, N_V, μ_{Band}, and N_{SD} were chosen to be 5×10^{18} [cm^{-3}], 5×10^{18} [cm^{-3}], 10 [$cm^2/V{\cdot}s$], and 2.3×10^{17} [cm^{-3}], respectively. Then, the GI trap parameters are extracted in the order of ΔE_T, σ_0, and N_{OT} as a unique set of parameters, whose values are adjusted by numerical iterations until all of simulated normalized $t_{sat,rec}(T)$, $t_{sat,rec}(T)$, and $\Delta V_{T,rec}(t)$ agree well with the measured ones in all PBTS temperatures under the conditions of specific error factor, significant digit, and proper range. When this agreement is accomplished with the proposed parameter-extraction procedure, all parameters (ΔE_T, σ_0, N_{OT}, and PF.B) can be extracted as a unique solution.

Finally extracted parameters were PF.B = $1 \times 10^{12}\,s^{-1}$, $N_{OT} = 2.6 \times 10^{18}\,cm^{-3}$, $\Delta E_T = 0.6$ eV, and $\sigma_0 = 3 \times 10^{-19}\,cm^2$. The line in Fig. 2(a) and the circle in Fig. 2(b) show our TCAD simulation results where our extracted parameters are used, which suggests that this parameter-based simulation reproduces the measured PBTS time-evolution of ΔV_T very well over a wide range of temperatures. Undoubtedly, Fig. 2(a) and (b) verify that our TCAD framework is well-calibrated and the values of extracted parameters are very reasonable.

4. Results and discussion

The bias-temperature-stress (BTS) time-evolution of the TFT ΔV_T is commonly modeled by the stretched-exponential function (SEF) as

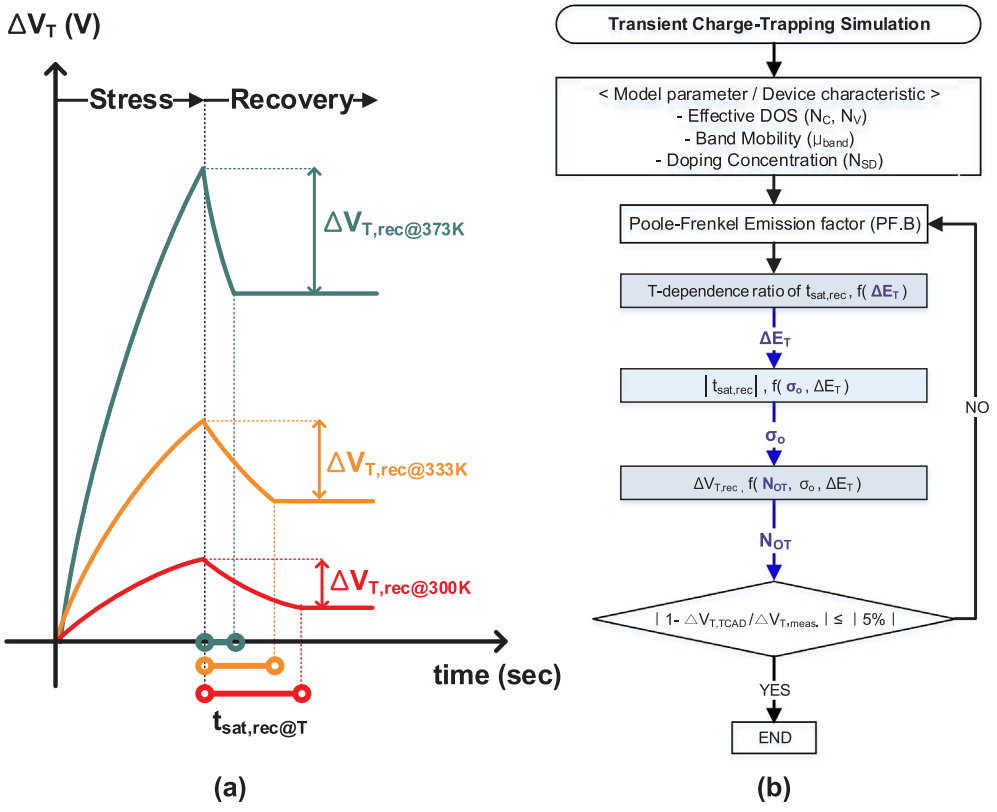

Fig. 3. (a) Time evolution of ΔV_T under the PBS/recovery condition with different temperatures. (b) Extraction procedure of electron trap parameter.

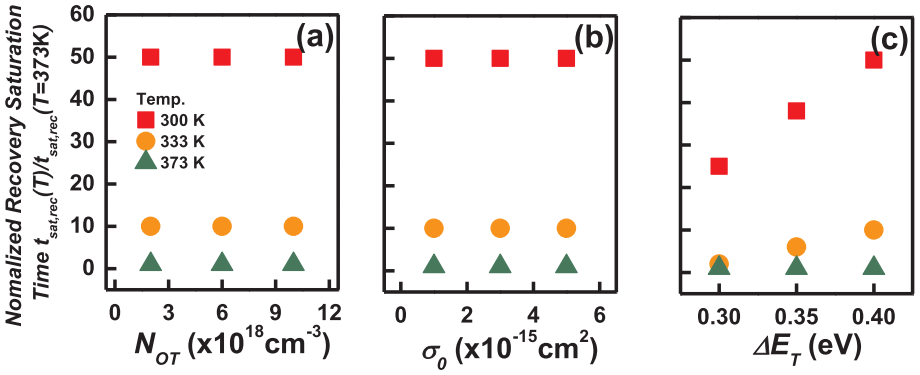

Fig. 4. Temperature-dependence ratio of recovery saturation time with variation of (a) N_{OT}, (b) σ_0 and (c) ΔE_T.

follows [16,17]:

$$\Delta V_T = \Delta V_{th0} \times \left[1-\exp\left(-\frac{t}{\tau}\right)^{\beta}\right] \quad (1)$$

where ΔV_{th0} is the ΔV_T at infinite time, τ is the characteristic time constant, and β is the stretching exponent with a value smaller than 1. The SEF for BTS/recovery has its own set of parameters, such as ΔV_{th0}, τ, and β, whose values are dependent on the BTS temperature T.

Consistently, in our case, the line in Fig. 2(b) shows that the PBTS time-evolution of ΔV_T is well fitted with SEF model (except the recovery time) for both the experimentally de-embedded ΔV_T (triangle) and the simulated one (circle). Our PBTS temperature-dependent SEF parameters are shown in Fig. 2(c), where the stress time can be much longer than the experimental test because the data are taken from TCAD simulation.

The activation energy E_a for BTS instability can be commonly acquired from the temperature dependence of the SEF parameter τ using the formula of $\tau = \tau_0 \times \exp(E_a/kT)$; E_a is frequently correlated with the identification of specific physical mechanisms. Therefore, for the quantitative analysis and joint-optimization of the GI and the IGZO film from the perspective of PBTS stability, it is very important to study how E_a individually depends on the electron trap parameter.

Thus, based on our well-calibrated TCAD simulation framework, the relationship between the GI electron trap parameters and the E_a of electron trapping in IGZO TFTs under PBTS was investigated more in detail, which is practically very important use of our parameter-extraction technique. As shown in Fig. 5(a) and (b), E_a increases with an increase of σ_0, whereas E_a is independent of N_{OT}. The N_{OT} increases only the absolute amount of electron trapping [12], but does not affect τ, so there is no N_{OT} dependence of E_a. The σ_0-dependent E_a increase occurs because when electron trapping is activated by σ_0, the temperature dependence of τ becomes more prominent [18–20]. However, the ΔE_T dependence of E_a suggests that there are two regimes different from each other; this is shown in Fig. 5(c). The former regime is the thermionic field emission-based electron trapping dominant regime, whereas the latter is the PF emission/hopping dominant regime. The two mechanisms are explained associated with the capture rate (c_n) [18–21] and emission rate (e_n) [22,23] as shown in Fig. 6. We express the c_n considering tunneling probability ($\underline{T}$) [24,25] and e_n as:

$$c_n = v_{th}\sigma_0 N_{OT}(1-f_T)N_s \underline{T} \times WLt_{inv} \quad (2)$$

$$e_n = PF.\ B \times \exp\left(-\frac{(3.75-\Delta E_T)-q\sqrt{qF/\pi\varepsilon}}{kT}\right) \approx PF.\ B \times \exp\left(-\frac{(3.75-\Delta E_T)-q\sqrt{qV_{GS}/T_{GI}\pi\varepsilon}}{kT}\right) \quad (3)$$

where v_{th} is the thermal velocity of electrons (units: cm/s), f_T is Fermi-Dirac distribution function in the GI trap, N_s is channel electron density considering PBTS condition (units: cm^{-3}), t_{inv} is channel thickness, q is the elementary charge of an electron, F is electric field in GI, and ε is the GI SiO_2 permittivity.

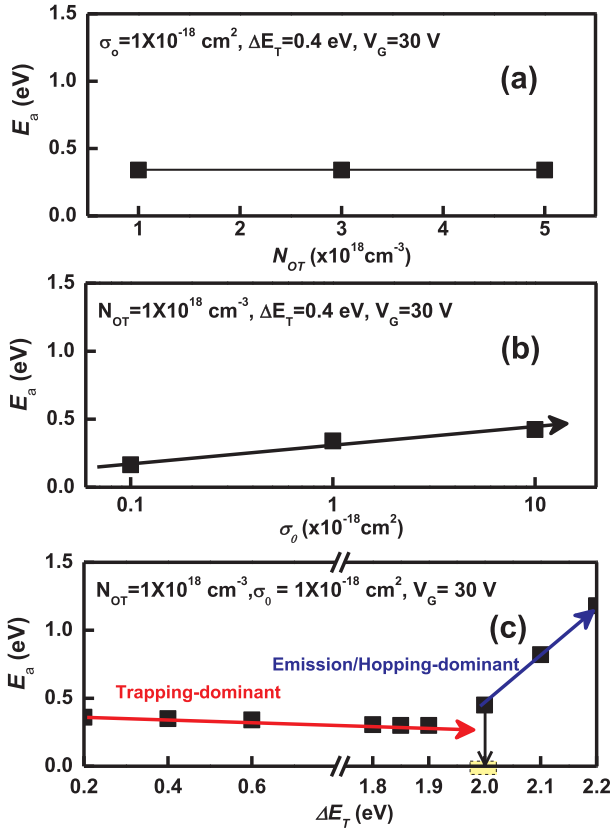

Fig. 5. Activation energy with variation of (a) N_{OT}, (b) σ_0 and (c) ΔE_T.

In the electron trapping dominant regime, the c_n decreases abruptly with an increase in ΔE_T because the energy distance between the E_T and the $E_{C,IGZO}$ increases as shown in Fig. 6(b), and the electron trapping becomes more difficult [18]. The E_a then decreases slightly because the decreased c_n causes a reduction in the temperature dependence of electron trapping.

In contrast, in the PF emission/hopping dominant regime, the e_n increases very abruptly with an increase in ΔE_T because the energy distance between the E_T and the $E_{C,GI}$ decreases; it becomes easier for electrons to hop further away from the GI/IGZO interface as shown in Fig. 6(a). The E_a then increases sharply (Fig. 5(c)) because the increased e_n increases the temperature dependence of electron hopping. Our finding shows that the critical ΔE_T between the two regimes in Fig. 5(c) eventually corresponds to the cross-over ΔE_T point wherein the ΔE_T -dependent c_n equals the ΔE_T -dependent e_n (Fig. 6(b)).

Finally, the PBTS voltage (V_{STR}) dependence is shown in Fig. 7(a). When the V_{STR} increases at a fixed ΔE_T, the E_a also increases because

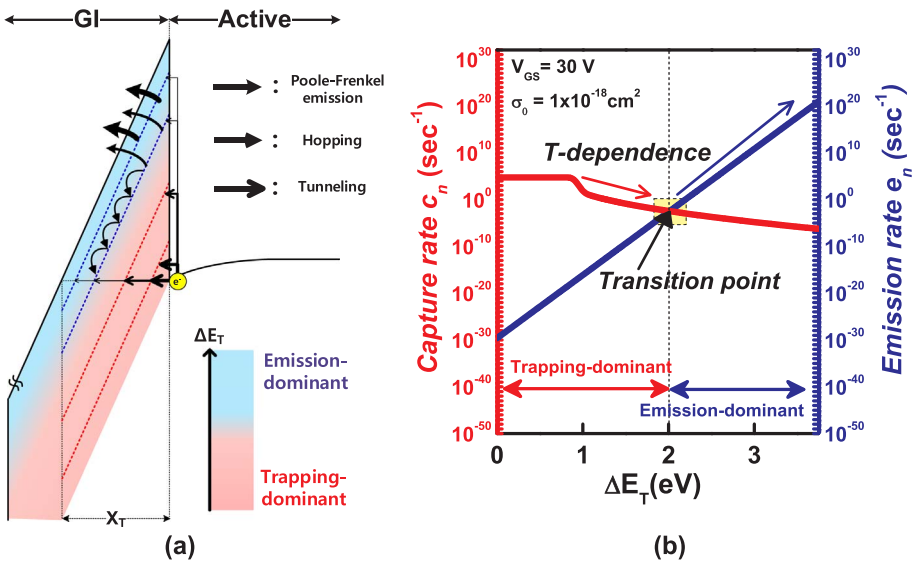

Fig. 6. (a) An energy band diagram explaining the mechanism of charge trapping and de-trapping such as PF emission, hopping and tunneling. (b) The ΔE_T-dependent c_n and e_n.

the temperature dependence of c_n increases (see Fig. 7(b)). In addition, the critical ΔE_T decreases with the increase of V_{STR} (see Fig. 7(c)) because the balance between c_n and e_n is obtained at a deeper E_T level from $E_{C,GI}$ as the V_{STR} increases. This provides a very important quantitative insight that the electric field dependence of the PF emission-based electron hopping is stronger than that of the thermionic field emission-based electron trapping.

5. Conclusion

Experimental extraction of the GI electron trap parameters which are only associated with charge trapping into GI under PBTS is proposed and its detailed procedure is demonstrated for the first time in a-IGZO TFTs. Our extraction technique is established by combining the PBTS/recovery time-evolution of the experimentally decomposed threshold voltage shift (ΔV_T) and the technology computer-aided design (TCAD)-based charge trapping simulation. Our parameters and TCAD simulation reproduced the measured PBTS time-evolution of ΔV_T very well over a wide range of temperatures. Furthermore, we found that E_a increases when σ_0 increases, whereas E_a is independent of N_{OT} by comprehensively investigating the relationship between the GI trap parameters and the E_a value. It was also found that to the cross-over ΔE_T point originates from the complicated T-dependent competition between c_n and e_n. The V_{STR} dependence of the relationship between E_a and ΔE_T proved that the electric field dependence of the PF emission-based electron hopping is stronger than that of the thermionic field emission-based electron trapping.

Our results are potentially useful for the quantitative analysis and

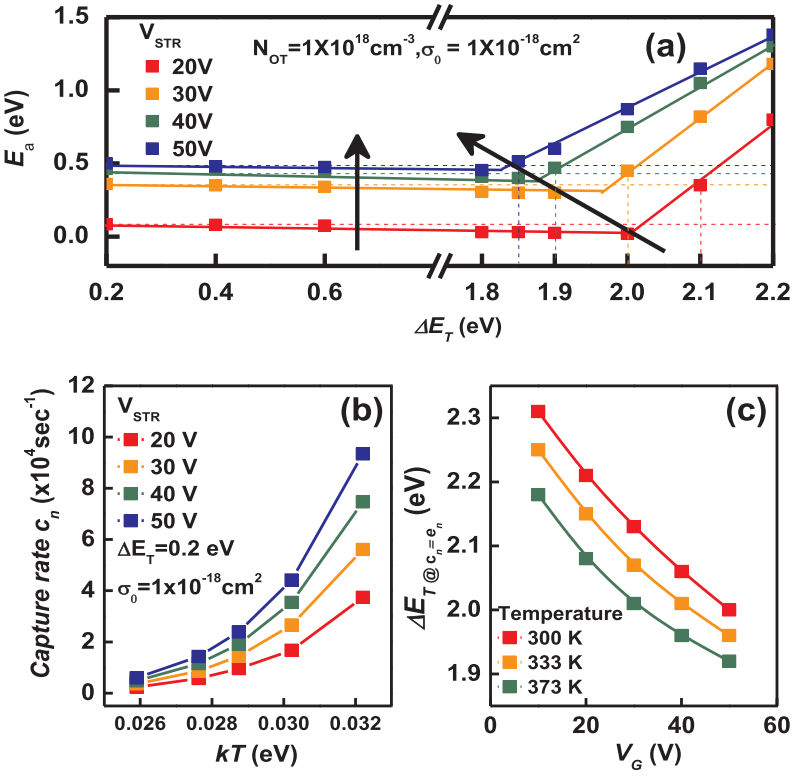

Fig. 7. (a) ΔE_T-dependent activation energy with V_{STR} variations, (b) temperature-dependent capture rate with V_{STR} variations, and (c) V_{STR} dependence of ΔE_T when c_n equal to e_n.

joint-optimization of the GI and the IGZO film for the TFT process integration in wearable healthcare monitoring systems and in display backplanes.

Acknowledgement

This work was supported by the National Research Foundation of Korea (NRF) Grant funded by the Korean Government (MSIP) under Grant 2016R1A5A1012966, in part by the Ministry of Science, ICT and Future Planning Grant 2015M3D1A1068061, and in part by the Ministry of Education, Science and Technology (MEST) Grant 2017R1A2B4006982.

References

[1] Ha C, Lee H, Kwon J, Seok S, Ryoo C-I, Yun K, et al. 69.2: distinguished paper : high reliable a-IGZO TFTs with self-aligned coplanar structure for large-sized ultrahigh-definition OLED TV. SID Symp Dig Tech Pap 2015;46:1020–2. http://dx.doi.org/10.1002/sdtp.10346.

[2] Yeh B, Lin C. High-performance 4K × 2K 65-in. TV with BCE-type oxide TFTs 2015:943–5.

[3] Kamiya T, Nomura K, Hosono H. Present status of amorphous In–Ga–Zn–O thin-film transistors. Sci Technol Adv Mater 2010;11:44305. http://dx.doi.org/10.1088/1468-6996/11/4/044305.

[4] Discrete JS, Nomura K, Ohta H, Takagi A, Kamiya T. Room-temperature fabrication of transparent flexible thin-film transistors using amorphous oxide semiconductors 2004;432:3383–6.

[5] Mativenga M, Choi MH, Choi JW, Jang J. Transparent flexible circuits based on amorphous-indium-gallium-zinc-oxide thin-film transistors. IEEE Electron Device Lett 2011;32:170–2. http://dx.doi.org/10.1109/LED.2010.2093504.

[6] Chien C-W, Wu C-H, Tsai Y-T, Kung Y-C, Lin C-Y, Hsu P-C, et al. High-performance flexible a-IGZO TFTs adopting stacked electrodes and transparent polyimide-based nanocomposite substrates. IEEE Trans Electron Devices 2011;58:1440–6. http://dx.doi.org/10.1109/TED.2011.2109041.

[7] Steudel S, van der Steen J-LPJ, Nag M, Ke TH, Smout S, Bel T, et al. Power saving through state retention in IGZO-TFT AMOLED displays for wearable applications. J Soc Inf Disp 2017. http://dx.doi.org/10.1002/jsid.544.

[8] Choi S, Jang J, Kang H, Baeck JH, Bae JU, Park K-S, et al. Systematic decomposition of the positive bias stress instability in self-aligned coplanar InGaZnO thin-film transistors. IEEE Electron Device Lett 2017;38:580–3. http://dx.doi.org/10.1109/LED.2017.2681204.

[9] Powell MJ. The physics of amorphous-silicon thin-film transistors. IEEE Trans Electron Devices 1989;36:2753–63. http://dx.doi.org/10.1109/16.40933.

[10] Lopes ME, Gomes HL, Medeiros MCR, Barquinha P, Pereira L, Fortunato E, et al. Gate-bias stress in amorphous oxide semiconductors thin-film transistors. Appl Phys Lett 2009;95:63502. http://dx.doi.org/10.1063/1.3187532.

[11] Oh S, Baeck JH, Bae JU, Park K-S, Kang IB. Effect of interfacial excess oxygen on positive-bias temperature stress instability of self-aligned coplanar InGaZnO thin-film transistors. Appl Phys Lett 2016;108:141604. http://dx.doi.org/10.1063/1.4945404.

[12] Wang LL, Liu TC, Yuying Cai, Shengdong Zhang. Thin-film transistor Vth shift model based on kinetics of electron transfer in gate dielectric. IEEE Trans Electron Devices 2014;61:1436–43. http://dx.doi.org/10.1109/TED.2014.2309980.

[13] Ling Wang L, Hongyu He, Xiang Liu, Wei Deng, Shengdong Zhang. Charge trapping model for temporal threshold voltage shift in a-IGZO TFTs considering variations of carrier density in channel and electric field in gate insulator. IEEE Trans Electron Devices 2015;62:2219–25. http://dx.doi.org/10.1109/TED.2015.2433681.

[14] Fomani AA. Threshold voltage instability and relaxation in hydrogenated amorphous silicon thin film transistors. M.S. thesis. Waterloo, ON, Canada: Dept. Electr. Comput. Eng., Waterloo Univ.; 2005.

[15] Atlas User's Manual, Silvaco; 2016.

[16] Libsch FR, Kanicki J. Bias-stress-induced stretched-exponential time dependence of charge injection and trapping in amorphous thin-film transistors. Appl Phys Lett 1993;62:1286–8. http://dx.doi.org/10.1063/1.108709.

[17] Lee J-M, Cho I-T, Lee J-H, Kwon H-I. Bias-stress-induced stretched-exponential time dependence of threshold voltage shift in InGaZnO thin film transistors. Appl Phys Lett 2008;93:93504. http://dx.doi.org/10.1063/1.2977865.

[18] Katsube T, Kakimoto K, Ikoma T. Temperature and energy dependences of capture cross sections at surface states in Si metal-oxide-semiconductor diodes measured by deep level transient spectroscopy. J Appl Phys 1981;52:3504–8. http://dx.doi.org/10.1063/1.329128.

[19] Ielmini D, Spinelli AS, Rigamonti MA, Lacaita AL. Modeling of SILC based on electron and hole tunneling. I. Transient effects. IEEE Trans Electron Devices 2000;47:1258–65. http://dx.doi.org/10.1109/16.842971.

[20] Mao L-F. Temperature dependence of the tunneling current in metal-oxide-semiconductor devices due to the coupling between the longitudinal and transverse components of the electron thermal energy. Appl Phys Lett 2007;90:183511. http://dx.doi.org/10.1063/1.2735929.

[21] Parker GH, Mead CA. The effect of trapping states on tunneling in metal-semiconductor junctions. Appl Phys Lett 1969;14:21–3. http://dx.doi.org/10.1063/1.1652641.

[22] Harrell WR, Frey J. Observation of Poole-Frenkel effect saturation in SiO_2 and other insulating films. Thin Solid Films 1999;352:195–204. http://dx.doi.org/10.1016/S0040-6090(99)00344-2.

[23] Jonscher AK, Loh CK. Poole-Frenkel conduction in high alternating electric fields. J Phys C: Solid State Phys 1971;4:1341–7. http://dx.doi.org/10.1088/0022-3719/4/11/009.

[24] Lenzlinger M, Snow EH. Fowler-Nordheim tunneling into thermally grown SiO_2. J Appl Phys 1969;40:278–83. http://dx.doi.org/10.1063/1.1657043.

[25] Kane EO. Theory of tunneling. J Appl Phys 1961;32:83–91. http://dx.doi.org/10.1063/1.1735965.